Published in final edited form as:
Langmuir. 2010 August 17; 26(16): 13407–13414. doi:10.1021/la102106t.

Structure and Dynamics of Cholic Acid and Dodecylphosphocholine-Cholic Acid Aggregates

Abdallah Sayyed-Ahmad, **Lenard M Lichtenberger**, and **Alemayehu A Gorfe***
Department of Integrative Biology and Pharmacology, The University of Texas Health Science Center at Houston, Houston, Texas 77030, USA

Abstract

Bile acids are powerful detergents that emulsify and solubilize lipids, vitamins, cholesterol and other molecules in the biliary tract and intestines. It has long been known that bile acids form soluble mixed micelles with lipids. However, the detailed thermodynamic and structural properties of these micelles are not fully understood. This study sheds light on this issue based on results from multiple molecular dynamics simulations of cholic acid (CA) and dodecylphosphocholine (DPC) mixed micelles. We found that CA molecules form aggregates of up to 12 monomers with a mean size of 5–6. In agreement with several previous simulations and earlier predictions, the overall shape of these CA clusters is oblate disk-like such that the methyl groups point toward the core of the aggregate and the hydroxyl groups point away from it. The self-aggregation behavior of the CA clusters in the DPC-CA mixture is similar to the pure CA. Furthermore, the sizes and aggregation numbers of the DPC-CA mixed micelles are linearly dependent on CA molarity. In agreement with the radial shell model of Nichols and Ozarowski [Nichols, J. W.; Ozarowski, J. *Biochemistry* **1990**, *29*, 4600][1], our results demonstrate that CA molecules form a wedge between the DPC molecules with their hydroxyl and carboxyl groups facing the aqueous phase while their methyl groups are buried in and face the hydrocarbon core of the DPC micelle. The DPC-CA micelles simulated here tend to be spherical to prolate in shape, with the deviation from spherical geometry significantly increasing with increasing CA:DPC ratio.

Keywords

bile acid; cholic acid; molecular dynamics; mixed micelles; phosphatidylcholine aggregation

1. Introduction

Bile is a digestive and excretory fluid secreted by hepatic parenchymal cells into the intestine of vertebrates. Its major constituents include bile acids (BAs), lipids and cholesterol. BAs are products of cholesterol metabolism. The most common primary BAs in human include cholic acid, deoxycholic acid and chenodeoxycholic acid. All share a significant structural similarity to cholesterol, as can be seen from the structure of cholic acid (CA) shown in Figures 1A &B. Although these metabolites are known to be powerful detergents, their chemical structure and physicochemical characteristics are very different from those of the common surfactants characterized by a hydrophilic head and a

*Corresponding Author: Alemayehu.G.Abebe@uth.tmc.edu, Phone: 713-300-7538, Fax: 713-500-7444.

Supporting Information Available

Analysis details for DPC-CA and CA aggregates characterization and identification. Time evolution of various structural parameters used to monitor and characterize pure CA and DPC-CA micelles. This information is available free of charge via the Internet at http://pubs.acs.org/.

hydrophobic tail. BAs are anionic and rigid bi-planar amphiphiles containing two methyl groups on the convex hydrophobic face and up to three hydroxyl groups on the concave hydrophilic face. They also have a flexible short hydrocarbon tail carrying a carboxyl and a methyl group. The facial amphipathicity of BA molecules allows them to aggregate and spontaneously form clusters among themselves and mixed micelles with lipids and cholesterol[2–4].

BAs play a crucial role in facilitating intestinal absorption of nutrients by solubilizing phospholipids such as phosphatidylcholine (PC) and other lipophilic molecules of diverse chemical structure, such as lipid soluble vitamins. Furthermore, their unique physicochemical properties made them valuable in the fields of drug development and drug delivery[5–7]. A prominent example for the successful application of BAs in therapeutics is their use (and specifically the hydrophilic BA, ursodeoxycholic acid) in the treatment of choleliths as agents to dissolve cholesterol gallstones[2]. However, BAs can also be toxic to the GI tract[8]. It has been proposed that the formation of BA mixed micelles with PC normally present in bile reduces the injurious effect of BAs on the mucosal lining of the small intestine[9–11]. As a result, BA aggregation and physiological function have been under intense experimental scrutiny for over a century[2,12,13]. A variety of techniques have been utilized to study BA and BA-PC aggregation, including small-angle neutron and X-ray scattering[14,15], quasi-elastic light scattering[16–18] and NMR spectroscopy[19–21]. These experiments led to the proposal of several different models of BA aggregation in vivo[3,4,22–24]. The most widely used and perhaps also the most intuitive model relies on the hydrophobic effect and hydrogen bonding to be the driving forces for the assembly of primary and secondary micelles, respectively.[25] According to this model, at low concentrations disk shaped primary micelles with one layer of BA molecules are formed by aligning their hydrophobic faces towards one another and their hydrophilic faces to the solvent. At higher concentrations, hydrogen bonding among the primary micelles leads to the formation of secondary micelles[25]. However, the detailed structural and thermodynamic properties of these aggregates are not fully characterized [3,4].

As noted above, BAs in the gallbladder and the small intestine form mixed micelles with PCs. There have been several proposed models of PC-BA mixed micelle aggregation, including the formation of spherical/globular, simple disk, mixed disk, rod-like and cylindrical shapes[16,26]. The PC-CA mixed micelles are now commonly believed to be spherical[26,27] or cylindrical[16,26] with the hydrophobic face of the BAs resting between the polar headgroups of the solubilized PCs[1].

Atomistic molecular dynamics (MD) simulations are theoretical techniques that are commonly used to gain insights into the aggregation processes of surfactants and other amphipathic molecules [28–33]. In the past decade, several MD simulation studies of BA micelles[34–37] have been published. However there has been only one MD simulation study on BA-PC mixture [38]. The simulations, carried out with a united atom force field, targeted a mixture of CA, cholesterol and palmitoyloleoylphosphatidylcholine (POPC) at 32:0:16 and 24:0:24 and 28:4:16 ratios. During the first 10 ns of each simulation, a large mixed micelle consisting of all the CA and POPC molecules was formed. This study provided useful insights into the structural and dynamic properties of these micelles. However, a systematic simulation study on, for example, the effect of variable concentration on the structure and thermodynamics of the aggregation of BA and PC-BA micelles has not been made. This is crucial because, in vivo, BA-to-PC mole fractions can be as high as 5 to 1, with the actual value varying with location (i.e. the gallbladder, bile duct or intestinal lumen) [8,39].

The present work aims at characterizing the aggregation dynamics and intermolecular interactions underlying the formation of dodecylphosphocholine (DPC)-CA mixed micelles.

The zwitterionic detergent DPC has been commonly used to mimic PCs due to its smaller size and faster relaxation times [38,39]. DPC and PC lipids have the same phosphocholine group, but the former have a single hydrocarbon tail and therefore spontaneously assemble into micelles instead of bilayers. We carried out all-atom MD simulations of pure CA and mixtures of a DPC micelle and CA at five different concentrations and mole fractions. To the best of our knowledge, these are the most extensive (total of 425 ns) PC-BA mixed micelle all-atom simulations performed to date spanning a range of CA and DPC concentrations. The results suggest that CA molecules form aggregates that predominantly consist of 5–6 monomers. In agreement with several previous simulations and earlier predictions, we found that the weight average aggregation number is between 3.54 and 5.89 while the overall shape of the CA clusters is oblate. In contrast to some previous reports, however, hydrogen bonding among CA primary micelles is weak and unstable. The self-aggregation behavior of the CA clusters is similar in the presence and absence of the DPC micelle. However, the CA molecules adsorb in a concentration dependent manner onto the surface of the DPC micelle with their hydroxyl groups facing the aqueous phase, and their hydrophobic side facing the center of the mixed micelle. Hydrogen bonding among the CA molecules and between CA and DPC plays an important role in stabilizing the DPC-CA mixed micelle, which adopted a globular/spherical to prolate shape with the deviation from spherical geometry being higher at larger CA-to-DPC ratio.

2. Methods

2.1. Initial structure and simulation setup

The starting coordinates for the solvated DPC micelle were derived from simulations by Wymore and co-workers[40], and used here after minimization and a short (~5ns) MD simulation. The micelle consisted of 60 DPC molecules and 4377 water molecules in a cubic box of size 56.15 Å, yielding a bulk water density of 0.033 $Å^{-3}$ away from the micelle-water interface.

During the initial setup of the pure CA and the DPC-CA simulations, the CA molecules were distributed randomly throughout the simulation box and in a spherical shell around the DPC micelle, respectively. Neutralizing sodium counterions were added in equal proportion to the CA molecules. To speed up the equilibration of the sodium ions, they were distributed randomly in a spherical shell of inner radius 3 Å and thickness 5 Å around the center of the two carboxyl oxygen atoms of the CA molecules. Each system was solvated in a cubic water box of edge length 100 Å or 72 Å (depending on the desired concentration as seen in Table 1). Overlapping water molecules were removed, yielding slightly different DPC concentrations in the different simulations (Table 1).

2.2. Molecular dynamics simulations

Initial bad atomic contacts among the CA molecules and/or between the DPC micelle core and water molecules were removed by minimizing the entire system for 100,000 steepest descent steps. To prevent penetration of water into the core of the DPC micelle during subsequent heating and equilibration steps, the first methyl carbon atoms (C_1 s) of the DPC molecules (see Figure 1C) were harmonically constrained by a quadratic potential with a spring constant, k, of 5 kcal mol^{-1} $Å^{-2}$. k was reduced by half every 0.5 ns during a 2 ns simulation period and then turned off.

The simulations were performed with the NAMD program[41] using the CHARMM general force field (CGenFF)[42] for CA and the CHARMM27 force field[43] for DPC. The short range van der Waals interactions were truncated at 12 Å, with a 14 Å cut-off used for the non-bonded list update. The long-range electrostatic interactions were calculated with the

particle mesh Ewald (PME) summation method with an FFT grid of approximately one point per angstrom. The NAMD multistep integrator was used to calculate bonded, non-bonded and electrostatic interactions at every 1, 2 and 4 fs, respectively. The temperature was set to the physiological value of 310 K and kept constant using Langevin dynamics with a damping coefficient of 10 ps^{-1}, whilst the Langevin piston method was utilized to maintain constant pressure of 1 atm with a piston period of 200 fs and decay time of 100 fs.

3. Results and discussions

Table 1 summarizes the seven simulations carried out at different water content and DPC-to-CA molar ratios. In the reference simulation, A, pure CA was simulated to obtain structural information and physical properties of CA micellar aggregates, while the rest of the simulations were carried out for DPC and CA mixtures at different DPC-to-CA ratios and concentrations.

3.1. CA self-assembly in the pure phase

Although the primary focus of the current work is on PC-CA micelles, we carried out a simulation of pure CA (simulation A) under the same condition as the PC-CA simulations to obtain a baseline for the aggregation behavior of the bile salts in DPC-CA mixtures.

A number of structure descriptors of CA clustering (see supplementary information), including the solvent accessible surface area (SASA), the number of CA monomers ($N_{Monomer}$), the weight and number aggregation numbers (N_W and N_N), and the number of CA aggregates of size n, (A_n, n>1) were monitored during the simulations. As the simulation progresses, the SASA and $N_{Monomer}$ drop sharply and stabilize after approximately 25 ns (Figures S1 A&B). Similarly N_W and N_N plateau after about 25 ns following a sharp rise in the beginning of the simulation (Figure S1C). The ensemble-averaged values of N_W and N_N computed from the last 20 ns of the simulation are 5.27±0.52 and 4.52±0.38, respectively. These aggregation numbers are in overall agreement with those reported by Coello and coworkers[44,45], who found $3.0 < N_W < 4.2$ for sodium cholate in the CA concentration ([CA]) range of 45 to 210 mM. Since N_W increases with [CA], these experimental results can only serve as a lower bound for our results, which were obtained at a higher [CA] of 270 mM. We note, however, that there are conflicting reports about the exact values of CA aggregation numbers (see Coello et al [44] for more details). Also, there is evidence that temperature and salinity nonlinearly affect the aggregation size of CA micelles[46]. Lastly, the ratio of N_W and N_N can be used as a measure of the polydispersity of the clusters[47]. In the current work, we find $\langle N_W \rangle / \langle N_N \rangle = 1.17$, suggesting that CA micellar aggregates are significantly polydisperse in size.

3.1.1. Structure of CA aggregates—Representative structures for the primary and secondary CA aggregates are illustrated in Figure 2. One can see that the hydroxyl and carboxyl groups are facing the aqueous phase while the hydrophobic methyl groups are facing each other, thus shielding themselves from water. A typical secondary CA aggregate such as the one shown in Figure 2B contains multiple hydrogen bonds (depicted in green dashed lines). However, unlike previous reports based on united atom force fields[34–37] the chain-like structures and inter-cluster hydrogen bonds are rare and unstable in the current work. On the other hand, similar to what was observed by Pártay and coworkers[35,36] and Warren et al[37], the primary CA aggregates have an oblate shape.

To further characterize the shape of the primary aggregates, the probability distribution of the angle (ε) between vectors $C_{18} \rightarrow C_{13}$ and the radial direction from the center of mass of each aggregate of size n ($2 \leq n \leq 9$) was determined by the normalized ε angle histograms (Figure 3). These histograms show that the most probable angle (representing 62–88% of the

data in each histogram) is less than 90° for all the aggregates. This implies that most CA molecules are oriented with their methyl groups pointing towards the core of the CA aggregate they belong to.

3.1.2. CA aggregate size distribution—The distribution of the ensemble-averaged number of CA aggregates of size n ($\langle A_n \rangle$, n>1) and the fraction of CA molecules ($\langle X_n \rangle$) that belong to these aggregates are shown in Figure 4. Apart from the ~ 9% that remained in solution as monomers, the majority of the CA molecules formed aggregates. Of these, ~50% formed aggregates of size 4–6 while another 22% formed dimers or trimers (Figure 4B). Thus, the CA aggregates can be characterized as polydisperse in size. Furthermore, $\langle X_n \rangle$ peaks at n = 5 (Figure 4B), clearly showing that CA clusters of size 5 are dominant. The larger clusters ($8 \leq n \leq 12$) tend to be significantly less stable. This is in contrast to previously reported simulations that yielded aggregation numbers as high as 31[37]. Nonetheless, our results not only support earlier findings that the spontaneously forming primary CA aggregates tend to adopt oblate disk-like structures that are mainly stabilized by hydrophobic interactions, but they are also consistent with the more recent measurements of weight average aggregation numbers [22,44,48].

3.2. DPC-CA micelle

3.2.1. Convergence of the DPC simulations—To establish whether the simulations are adequately equilibrated and observables of interest are sampling a stationary distribution, we investigated the effects of the simulation length, initial configuration and system size by monitoring several quantities (see supplementary information), such as SASA, R_{gyr} and number of CA adsorbed on the DPC micelle (N_{ads}). Figure S2A shows the time evolution of SASA for simulations B, C, D and E listed in Table 1. In each case, SASA drops sharply in the first 5–10 ns of the trajectories and becomes fully equilibrated after 10–30ns. The large initial drift in the SASA is due to the burial of the hydrophobic surface of the CA molecules as waters adjacent to their hydrophobic face are released. The time required for equilibration is clearly dependent on the DPC:CA molar ratio, with the lower the ratio the longer the relaxation time. To check whether the apparently fast equilibration is not due to the system being trapped in a local minimum, one of the systems (simulation C with a 1:1 DPC:CA mixture) was run for roughly twice the duration of the rest of the simulations. Figure S2A shows that there is no further drift in SASA. The same conclusions could be reached from the behavior of other structure descriptors such as N_{ads} and R_{gyr} (Figure S2B and S2C). These results show that equilibrium structural properties of the micelles can be reliably determined from the last 20 ns data of each simulation.

Because the initial distribution of the CA molecules around the DPC micelle was random, it is important to ensure that the choice of a particular initial configuration does not influence the outcome of the simulations. This was tested by repeating simulation C with all but the initial organization of the CA molecules around the DPC micelle unchanged (termed simulation C′). Figures S2 D–F compare simulations C and C′ in terms of SASA, R_{gyr} and N_{ads}. The results clearly show that despite fluctuations and initial differences, each of these parameters equilibrated to nearly identical values in the two simulations. This allows us to conclude that the results discussed below are robust with respect to initial configurations.

Finally, the size of the simulation system can in some cases affect simulation outcomes, especially for highly charged systems such as those in this study. Furthermore, changes in volume alter the concentration of the solute. We therefore investigated the effect of the simulation box size by running a third copy of simulation C (C″) after reducing the box volume roughly by half. Figures S2 D–F show that, indeed, the higher concentration of CA in simulation C″ leads to changes in the rate and size of CA aggregation and adsorption on

the DPC micelle. Compared with simulation C, the aggregation process in C″ is slow and the number of CA molecules adsorbed on the DPC micelle is high although no significant changes were detected in the more global SASA and R_{gyr}. In each case, however, equilibration was achieved within about 30ns.

3.2.2. CA self-assembly in the presence of a DPC micelle—The self-assembly behavior of the CA molecules in the presence of the DPC micelle is similar to those discussed above for the pure CA at comparable concentrations. For example, N_W for simulation C (which has the same number of CA molecules as that of simulation A) is ~5, which is the same as that from simulation A. Moreover, N_W and N_N derived from simulation B, C, D and E converged after 30 ns (Figure S3), exhibiting the same convergence behavior as the pure CA simulation. We also monitored the formation of CA aggregates of all sizes (n=2,3,…,12) that appear in the simulations as a function of time. As an example, we plotted $A_{n=1,2,\ldots,8}$ for simulation B (Figure S4), which contains the highest [CA]. Each one of the A_n plots converged rather quickly, with the slowest (A_6) converging after 30ns.

The final average values for N_W and N_N calculated from the last 20 ns of simulations B, C, D and E are (5.89±0.40, 4.95±0.33), (5.16±0.51, 4.47±0.44), (3.91±0.53, 3.54±0.55) and (3.68±0.43, 3.59±0.51), respectively. The corresponding "polydispersity indices" (i.e. $\langle N_W \rangle / \langle N_N \rangle$)[47] are 1.19, 1.15, 1.1 and 1.02. These values clearly show that the CA aggregates are polydisperse in size, especially at higher concentrations. Note that the polydispersity for simulation C (which has the same number of CA molecules as simulation A) is very close to that of the pure CA simulation (1.15 vs 1.17).

Figure 5A plots the distribution of the average number of CA aggregates ($\langle A_n \rangle$)of sizes n= 2,3,…,12 derived from simulation B while Figure 5B plots the fraction of CA molecules ($\langle X_n \rangle$) belonging to these aggregates. The profiles of the two distributions are very similar to the corresponding distributions for the pure CA simulation (Figure 4). However, the distribution in Figure 5 peaked at aggregate size of 6 instead of 5. This is due to the higher total concentration of CA rather than the presence of the DPC micelle. Taken together, these data clearly demonstrate that the presence of the DPC micelle did not appreciably alter the self-aggregation behavior of the CA molecules.

3.2.3. Dependence of DPC-CA assembly, size and shape on CA concentration —The ensemble-averaged radius of gyration of the DPC-CA micelle ($\langle R_{gyr} \rangle$) as a function of [CA] is shown in Figure 6A. At [CA] ≈ 66mM, $\langle R_{gyr} \rangle$ = 17.05±0.12 Å, which is not much different from the radius of gyration of the pure DPC micelle reported by Wymore and coworkers[40], reflecting the small number of CA molecules adsorbed onto the DPC micelle (see Figure 6B). $\langle R_{gyr} \rangle$ increases linearly with [CA] in the concentration range studied here, reaching 18.24±0.13 Å for [CA] ≈ 283 mM. Similarly, the average number of CA molecules adsorbed onto the DPC micelle ($\langle N_{ads} \rangle$) is a linear function of [CA] (Figure 6B).

The average ratios of the first principal moment of inertia (I_1) to the second (I_2) and to the third (I_3) principal moments of inertia are reported in Figure 6C. Wymore et al.[40] reported a I_1:I_2:I_3 ratio of 1.2:1.1:1 for the pure DPC micelle, not significantly different from our results of 1.17:1.08:1 at the relatively low [CA] of 66 mM. A more significant change in shape occurs in simulation B with the higher [CA] (283 mM), where the principal moments of inertia ratio becomes 1:3:1.1:1. This ratio leaves no doubt that the DPC-CA micelle is prolate in shape, especially at the higher CA concentrations studied here. In the following sections, the details of the aggregation mechanism and the DPC-CA micelle structural properties will be discussed based on the results from simulation B, which, owing to its high CA-to-DPC ratio, yielded the largest $\langle N_{ads} \rangle$, $\langle R_{gyr} \rangle$ and I_1/I_3.

3.2.4. Internal structure of the DPC-CA micelle—Figure 7A shows a representative structure of a water and ion striped snapshot with the single globular DPC-CA micelle in the center surrounded by many CA aggregates of different sizes and shapes. The adsorbed CA molecules are shown in ice blue while the secondary shell and bulk CA are shown in gray and lime green, respectively. Note that, in all of our simulated systems, the DPC micelle remained intact with no DPC molecule diffusing to the bulk. Since the behavior of the CA aggregates in the bulk solvent has been discussed in the previous section, here we focus only on those CAs that are adsorbed on the DPC micelle.

To characterize the internal structure of the DPC-CA micelle, we constructed a radial probability function,

$$\Omega_\alpha(r)=\frac{4\pi r^2\rho_\alpha(r)}{N_\alpha}, \quad (1)$$

which quantifies the probability of finding a given atom α at a given distance, r, from the center of mass of the DPC-CA micelle. $\rho_\alpha(r)$ is the number density and the normalization factor, N_α, is the total number of atoms of type α in the system, respectively.

The radial probability functions, $\Omega_\alpha(r)$, for α = C_1, C_6, C_{12}, N and P of DPC molecules indicate that they peak approximately at 18, 14, 9, 20 and 22 Å away from the center of mass of the DPC-CA micelle (Figure 7B). $\Omega_\alpha(r)$ for α = C_{18}, C_{19}, O_7, O_{12} and the carboxyl group of the CA molecules peak approximately at 16, 16, 20, 20 and 23 Å, respectively. Comparing the position of the peaks for $\Omega_{C_1}(r)$ and $\Omega_{C_6}(r)$ of DPC with $\Omega_{C_{18}}(r)$ and $\Omega_{C_{19}}(r)$of CA, one can clearly see that the two distributions overlap. In fact, $\Omega_{C_1}(r)$, $\Omega_{C_{18}}(r)$ and $\Omega_{C_{19}}(r)$ populate the same range of distances from the center of mass of the mixed micelle. Thus the methyl groups of the CA molecules (C_{18} and C_{19}) are immersed in the hydrocarbon region of the DPC micelle, encompassing C_1 and C_6 of DPC but never penetrating the hydrocarbon core of the micelle beyond the C_6 atoms of DPC. In contrast, the hydroxyl (e.g. O_7 and O_{12}) and the carboxyl groups are interacting with the headgroup near the P and N atoms of DPC. In addition, Na^+ ion distribution has a significant overlap with the CA carboxyl group distribution and some overlap with the hydroxyl group distributions, indicating that Na^+ ions are effectively screening the electrostatic repulsions between surface-bound CA molecules.

We examined the orientation of the CA rings with respect to the surface of the DPC-CA micelle by computing the order parameter $\langle\cos\varphi\rangle$, where φ is the mean angle between the vectors $M_{center} \rightarrow C_{10}$ and $C_{19} \rightarrow C_{10}$, and the vectors $M_{center} \rightarrow C_{13}$ and $C_{18} \rightarrow C_{13}$ (M_{center} is the center of the mixed micelle). Note that the vectors $M_{center} \rightarrow C_{10}$ and $M_{center} \rightarrow C_{13}$ are along the radial direction approximately normal to the micelle surface and $C_{18} \rightarrow C_{13}$ and $C_{19} \rightarrow C_{10}$ are along the respective bonds from the methyl groups to the rings.

To determine the orientation of CA molecules when they are (i) adsorbed to the mixed micelle surface, (ii) at the micelle-water interface and (iii) in bulk, we plotted $\langle\cos\varphi\rangle$ as a function of the distance of C_{13} or C_{10} of CA from the center of mass of the mixed micelle; $\langle\cos\varphi\rangle \gg 0$ means that the hydrophobic face of the CA molecules is pointing toward the center of the DPC-CA micelle. Figure 7C shows that the preferential organization of the CA molecules on the DPC micelle (r< 23 Å) is such that C_{13} — C_{18} and C_{10} — C_{19} form approximately 53° ($\langle\cos\varphi\rangle$ ~ 0.6) angle with the surface of the micelle. We conclude that on average, CA molecules are oriented with their methyl groups pointing towards the hydrocarbon core when they are adsorbed to the DPC-CA micelles. The plot also shows that CA aggregates at the micelle-water interface (23 Å ≤ r ≤ 40 Å) form a secondary shell and

interact with the DPC micelle with their methyl groups pointing away from the hydrocarbon core. This is due to interactions between the hydroxyl groups of CA aggregates and the headgroups of DPC or between the hydroxyl groups of the adsorbed CA molecules and those on the secondary shell (see Figure 7A). As expected $\langle \cos \varphi \rangle$ vanishes to zero for CA molecules far from the mixed micelle-water interface. Note that for $r < 12$ Å, the statistics is poor because there are fewer CA molecules that penetrate the micelle. Taken as a whole, the orientational analysis quantitatively demonstrates that CA molecules are oriented with their long axis parallel to the surface of the mixed micelle and their hydrophobic side facing the interior while their hydroxyl groups interact with the aqueous phase.

Once adsorbed on the DPC micelle, CA molecules stably bind to the DPC largely due to vdW interactions via their methyl groups (C_{18} and C_{19}). However, the DPC-CA micelle is also stabilized by hydrogen bonding between CA hydroxyl groups and the headgroup of DPC as well as by hydrogen bonds among the CA molecules themselves (Figure 8). The ratio of the average number of hydrogen bonds between CA and DPC molecules to the average number of adsorbed CA molecules was calculated to be 0.55, 0.65, 0.60 and 0.68 for simulation B, C, D and E, respectively. These ratios strongly suggest that hydrogen bonding between CA and DPC molecules play an important role in stabilizing the DPC-CA micelle.

4. Conclusions

The self-aggregation of BAs and their formation of mixed micelles with PCs are associated with their main physiological functions and have significant implications in health and disease. In the current work we were interested in how BAs associate with preformed lipid micelles rather than the assembly process per se. We therefore carried out simulations of preformed DPC micelle and CA mixtures at different concentrations and molar ratios. In addition, we carried out a simulation of pure CA to study the aggregation behavior of CA in the absence of a DPC micelle. Although a rigorous analysis of the thermodynamics of DPC-CA and CA micelle formation is needed to determine the relative contribution of each component of the aggregation free energy, our results indicate that the hydrophobic effect is the main driving force for the assembly of DPC-CA and CA micelles in aqueous media. This conclusion is based on the observation that as CA molecules aggregate, the hydrophobic surface area of CA molecules is reduced. This reduction is accompanied by the release of water molecules adjacent to the hydrophobic face of CA molecules. Our simulations also revealed that CA molecules form aggregates of up to 12 monomers, but aggregate sizes of 4–6 dominate. The CA aggregates have oblate disk-like shapes and are polydisperse in size; the calculated weight average aggregation numbers varied between 3.54 and 5.89. Furthermore, hydrogen bonding across primary CA aggregates was found to be weak and unstable.

The CA molecules adsorbed onto the DPC micelle are oriented with their hydrophobic face directed towards the hydrocarbon core of the DPC micelle. In fact, the methyl groups of the CA rings are immersed in the hydrocarbon core of the DPC micelle, while the hydroxyl and carboxyl groups are both interacting with the DPC headgroups and sodium counterions. These results support the proposed radial shell model of Nichols and Ozarowski[1]. In this model, cylindrical PC-BA micelles are formed with BA molecules filling the space between the PC headgroups with their long axis parallel to the mixed micelle axis and their methyl groups pointing toward the axis while their hydroxyl groups are pointing away from it. This organization is also supported by our findings that hydrogen bonding between CA and DPC molecules stabilize the DPC-CA micelle with approximately 0.5 hydrogen bonds per adsorbed CA molecule. A mixture of cholic acid and dioleoylphosphatidylcholine assembled into the same overall structure as described above during a 100ns simulation (Sayyed-

Ahmad and Gorfe, unpublished), suggesting the robustness of the above conclusions with respect to lipid type and composition.

Finally, we would like to point out that the results discussed in this report establish a foundation for a systematic thermodynamic study of PC-BA mixtures and BA aggregation, as well as the effect of BA on cellular lipid bilayers. This is of particular interest because detailed atomistic understanding of BA aggregation behavior is crucial for drug development and determination of drug bioavailability, cytotoxicity and side effects [37,49–51]. For example, nonsteroidal anti-inflammatory drugs (NSAIDs) are thought to cause injury to the intestine due to their interaction with PC-BA mixed micelles, perhaps resulting in abnormally high concentrations of cytotoxic monomeric BAs or the formation of NSAID-BA mixed micelles that have increased GI toxicity[8,52]. We are currently investigating the effect of selected NSAIDs on the aggregation of BA and PC mixtures.

Supplementary Material

Refer to Web version on PubMed Central for supplementary material.

Acknowledgments

This work is supported in part by a start up fund from the Medical School at the University of Texas Health Science Center at Houston and the NIH challenge grant IRC DK086304. We gratefully acknowledge computational resources support from TACC, NCSA and ORNL.

Abbreviations

BA	Bile Acid
CA	Cholic Acid
DPC	dodecylphosphocholine
POPC	palmitoyloleoylphosphatidylcholine
PC	phosphatidylcholine
SASA	Solvent accessible surface area
MD	molecular dynamics

References

1. Nichols JW, Ozarowski J. Biochemistry. 1990; 29:4600. [PubMed: 2372545]
2. Hofmann AF, Roda A. Journal of Lipid Research. 1984; 25:1477. [PubMed: 6397555]
3. Small, DM. Molecular Association in Biological and Related Systems. AMERICAN CHEMICAL SOCIETY; WASHINGTON, D. C: 1968. Size and Structure of Bile Salt Micelles; p. 31
4. Small D, Penkett S, Chapman D. Biochim Biophys Acta. 1969; 176:178. [PubMed: 5766016]
5. Simõesa SI, Marquesa CM, Cruza MEM, Cevcb G, Martins MBF. European Journal of Pharmaceutics and Biopharmaceutics. 2004; 58:509. [PubMed: 15451525]
6. Michael S, Thölea M, Dillmanna R, Fahrb A, Drewec J, Fricker G. European Journal of Pharmaceutical Sciences. 2000; 10:133. [PubMed: 10727879]
7. Garidel, P.; Lasch, J. Mixed Vesicles and Mixed Micelles: Formation, Thermodynamic Stability. In: Gregoriadis, G., editor. Liposome Technology: Liposome preparation and related techniques. Informa Healthcare; New York: 2007.
8. Petruzzellia M, Vaccaa M, Moschettaa A, Sassoa RC, Palascianoa G, Erpecumb KJv, Portincasaa P. Clinical Biochemistry. 2007; 40:503. [PubMed: 17321514]
9. Hofmann AF. News in Physiological Sciences. 1999; 14:24. [PubMed: 11390813]

10. Hofmann AF, Mysels K. Colloids Surfaces. 1988; 30:145.
11. Monte MJ, Martin JJ, Antelo A, Vazquez-Tato J. World Journal of Gastroenterology. 2009; 15:804. [PubMed: 19230041]
12. Forker EL. Annual Review of Physiology. 1977; 39:323.
13. Hofmann AF, Small DM. Annual Review of Medicine. 1967; 18:333.
14. Hjelm RP, Schteingart CD, Hofmann AF, Thiyagarajan P. The Journal of Physical Chemistry B. 1999; 104:197.
15. Zakrzewska J, Markovic V, Vucelic D, Feigin L, Dembo A, Mogilevsky L. The Journal of Physical Chemistry. 1990; 94:5078.
16. Cohen DE, Thurston GM, Chamberlin RA, Benedek GB, Carey MC. Biochemistry. 1998; 37:14798. [PubMed: 9778354]
17. Mazer NA, Carey MC. Biochemistry. 1983; 22:426. [PubMed: 6824637]
18. Mazer NA, Carey MC, Kwasnick RF, Benedek GB. Biochemistry. 1979; 18:3064. [PubMed: 465453]
19. Campredon M, Quiroa V, Thevand A, Allouche A, Pouzard G. Magnetic Resonance in Chemistry. 1986; 24:624.
20. Gouin S, Zhu XX. Langmuir. 1998; 14:4025.
21. Saitŏ H, Sugimoto Y, Tabeta R, Suzuki S, Izumi G, Kodama M, Toyoshima S, Nagata C. The Journal of Biochemistry. 1983; 94:1877.
22. Coello A, Meijide F, Núñez ER, Tato JV. Journal of Pharmaceutical Sciences. 1996; 85:9. [PubMed: 8926591]
23. Carey MC, Small DM. Archives of Internal Medicine. 1972; 130:506. [PubMed: 4562149]
24. Kawamura H, Murata Y, Yamaguchi T, Igimi H, Tanaka M, Sugihara G, Kratohvil JP. The Journal of Physical Chemistry. 1989; 93:3321.
25. Martin CC, Donald MS. The American journal of medicine. 1970; 49:590. [PubMed: 4924587]
26. Gantz DL, Wang DQH, Carey MC, Small DM. 1999; 76:1436.
27. Hofmann A, Hagey L. Cellular and Molecular Life Sciences. 2008; 65:2461. [PubMed: 18488143]
28. Jorge M. Langmuir. 2008; 24:5714. [PubMed: 18454560]
29. Tieleman DP, van der Spoel D, Berendsen HJC. The Journal of Physical Chemistry B. 2000; 104:6380.
30. Chowdhary J, Ladanyi BM. The Journal of Physical Chemistry B. 2009; 113:15029. [PubMed: 19842706]
31. Shang BZ, Wang Z, Larson RG. The Journal of Physical Chemistry B. 2009; 113:15170. [PubMed: 19905021]
32. Sammalkorpi M, Karttunen M, Haataja M. The Journal of Physical Chemistry B. 2007; 111:11722. [PubMed: 17877384]
33. Bogusz S, Venable RM, Pastor RW. The Journal of Physical Chemistry B. 2001; 105:8312.
34. Pártay LB, Sega M, Jedlovszky P. Langmuir. 2008; 24:10729. [PubMed: 18767819]
35. Pártay LB, Sega M, Jedlovszky P. Langmuir. 2007; 23:12322. [PubMed: 17944496]
36. Pártay LB, Jedlovszky P, Sega M. The Journal of Physical Chemistry B. 2007; 111:9886. [PubMed: 17661512]
37. Warren DB, Chalmers DK, Hutchison K, Dang W, Pouton CW. Colloids and Surfaces A: Physicochem Eng Aspects. 2006; 280:182.
38. Marrink SJ, Mark AE. Biochemistry. 2002; 41:5375. [PubMed: 11969397]
39. Gallaher D, Schneeman BO. American journal of physiology-Gastrointestinal and liver physiology. 1986; 250:G420.
40. Wymore T, Gao XF, Wong TC. Journal of Molecular Structure. 1999; 485–486:195.
41. James CP, Rosemary B, Wei W, James G, Emad T, Elizabeth V, Christophe C, Robert DS, Laxmikant K, Klaus S. Journal of Computational Chemistry. 2005; 26:1781. [PubMed: 16222654]
42. Vanommeslaeghe K, Hatcher E, Acharya C, Kundu S, Zhong S, Shim J, Darian E, Guvench O, Lopes P, Vorobyov I, Mackerell AD. Journal of Computational Chemistry. 2009; 9999 NA.

43. MacKerell AD, Bashford D, Bellott M, Dunbrack RL, Evanseck JD, Field MJ, Fischer S, Gao J, Guo H, Ha S, Joseph-McCarthy D, Kuchnir L, Kuczera K, Lau FTK, Mattos C, Michnick S, Ngo T, Nguyen DT, Prodhom B, Reiher WE, Roux B, Schlenkrich M, Smith JC, Stote R, Straub J, Watanabe M, Wiorkiewicz-Kuczera J, Yin D, Karplus M. J Phys Chem B. 1998; 102:3586.

44. Coello A, Meijide F, Rodriguez Nunez E, Vazquez Tato J. The Journal of Physical Chemistry. 1993; 97:10186.

45. Adela C, Francisco M, Eugenio Rodríguez N, Jose Vázquez T. Aggregation behavior of bile salts in aqueous solution. 1996; 85:9.

46. Sugioka H, Matsouka K, Moroi Y. Journal of Colloid Interface Science. 2003; 259:156.

47. Lazaridis T, Mallik B, Chen Y. The Journal of Physical Chemistry B. 2005; 109:15098. [PubMed: 16852911]

48. Hao L, Lu R, Leaist D, Poulin P. Journal of Solution Chemistry. 1997; 26:113.

49. Muranushi N, Kinugawa M, Nakajima Y, Muranishi S, Sezaki H. International Journal of Pharmaceutics. 1980; 4:271.

50. Muranishi S, Muranushi N, Sezaki H. International Journal of Pharmaceutics. 1979; 2:101.

51. Stenberg P, Bergström CAS, Luthman K, Artursson P. Clinical Pharmacokinetics. 2002; 24:877. [PubMed: 12190333]

52. Barrios JM, Lichtenberger LM. Gastroenterology. 2000; 118:1179. [PubMed: 10833493]

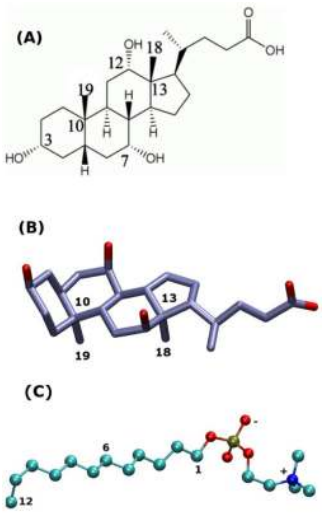

Figure 1.

Structures of the bile acid and phospholipid molecules used in this study. The chemical (A) and 3-dimensional (B) structures of cholic acid (3-alpha,7-alpha,12-alpha-trihydroxy-5-beta-cholan-24-oic acid) with standard numbering. In (B), oxygen and carbon atoms are in red and ice blue, respectively. (C) A CPK representation of a DPC molecule with carbon, oxygen, nitrogen and phosphorous atoms in cyan, red, blue and olive, respectively. In (B) and (C) hydrogen atoms are omitted for clarity.

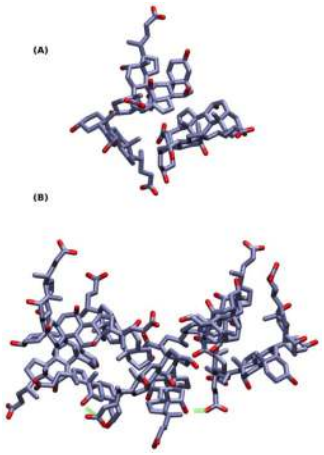

Figure 2.
Snapshots of cholic acid aggregates. Examples of typical primary (A) and secondary (B) CA aggregates formed during the simulation of pure CA. Notice that the hydroxyl and carboxyl groups face the aqueous phase (outwards) while the hydrophobic methyl groups face each other (inwards). Hydrogen bonds are shown in green dashed lines.

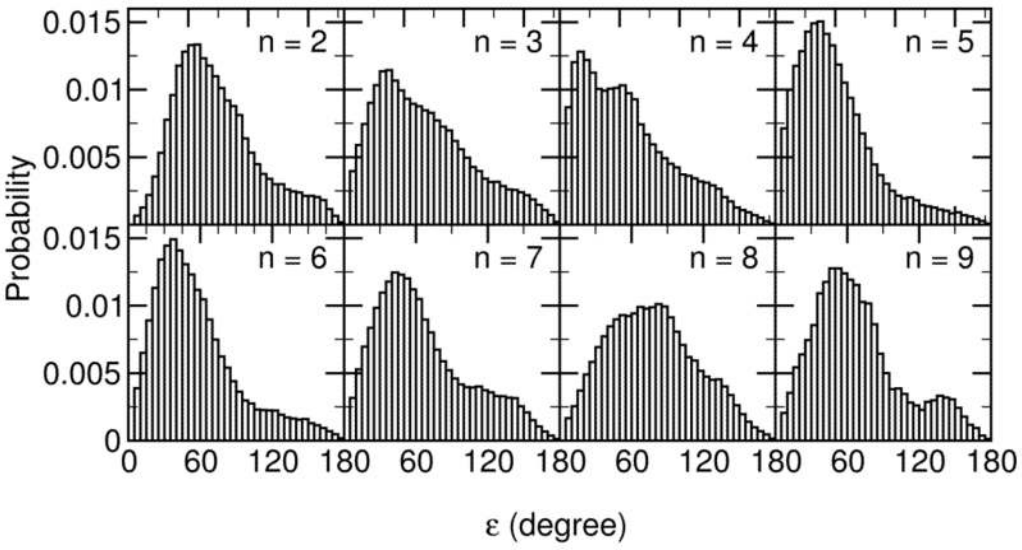

Figure 3.
Normalized histograms of the angle ε between $C_{18} \rightarrow C_{13}$ and the radial direction from the center of mass for each aggregate of size n ($2 \leq n \leq 9$).

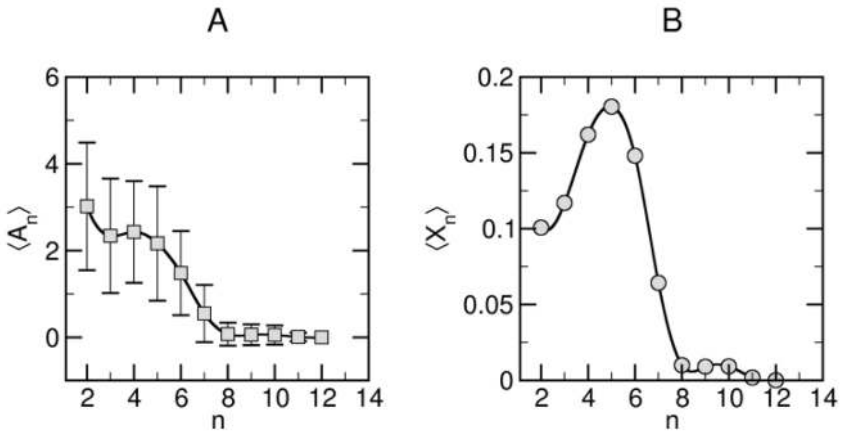

Figure 4.

Ensemble-averaged thermodynamic properties of CA clusters derived from the simulation of pure CA. Distributions of the numbers of clusters ($\langle A \rangle_n$) and the fraction of CA molecules ($\langle X_n \rangle$) belonging to cluster size n ($n \geq 2$). All ensemble-averaged properties in this and subsequent figures were calculated from the last 20 ns of the simulations. Error bars represent one standard deviation. Note that the numbers of aggregates of sizes less than 7 have higher fluctuations because they are in dynamic equilibrium with one another and because the absolute magnitude of the fluctuations depends on the total count of a given cluster (see Fig S4).

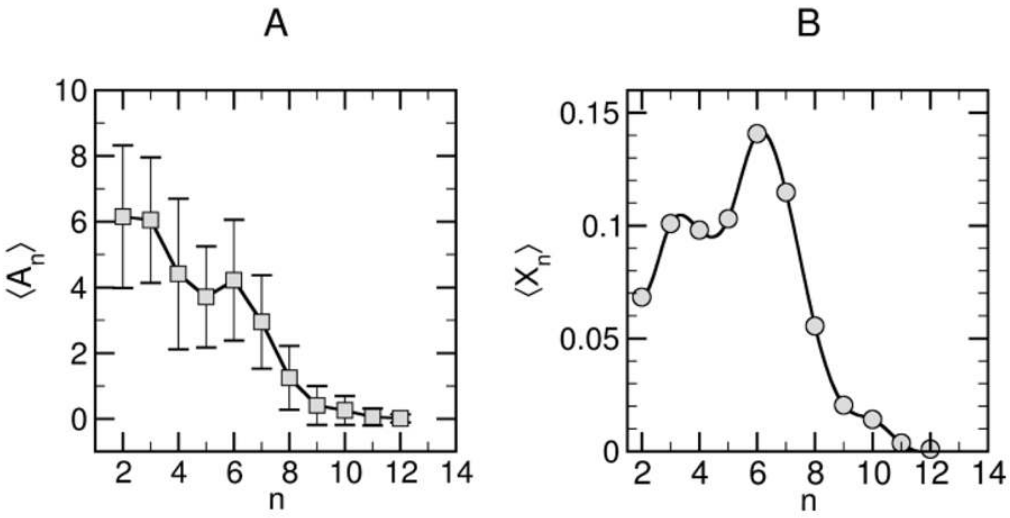

Figure 5.

Ensemble-averaged thermodynamic properties of CA clusters derived from simulation B. (A) Size ($\langle A_n \rangle$) and (B) mole fraction ($\langle X_n \rangle$) distributions of aggregates of different sizes.

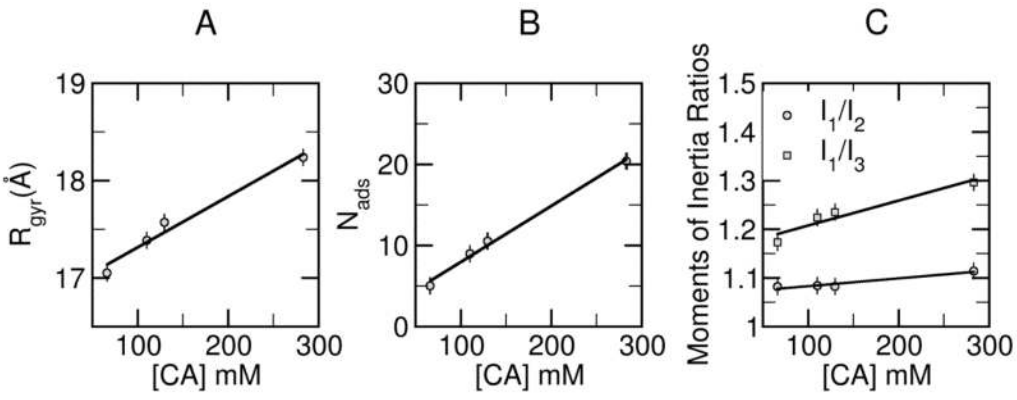

Figure 6.
(A) R_{gyr}, (B) N_{ads} and (C) I_1/I_2 and I_1/I_3 as a function of [CA] (see text for details).

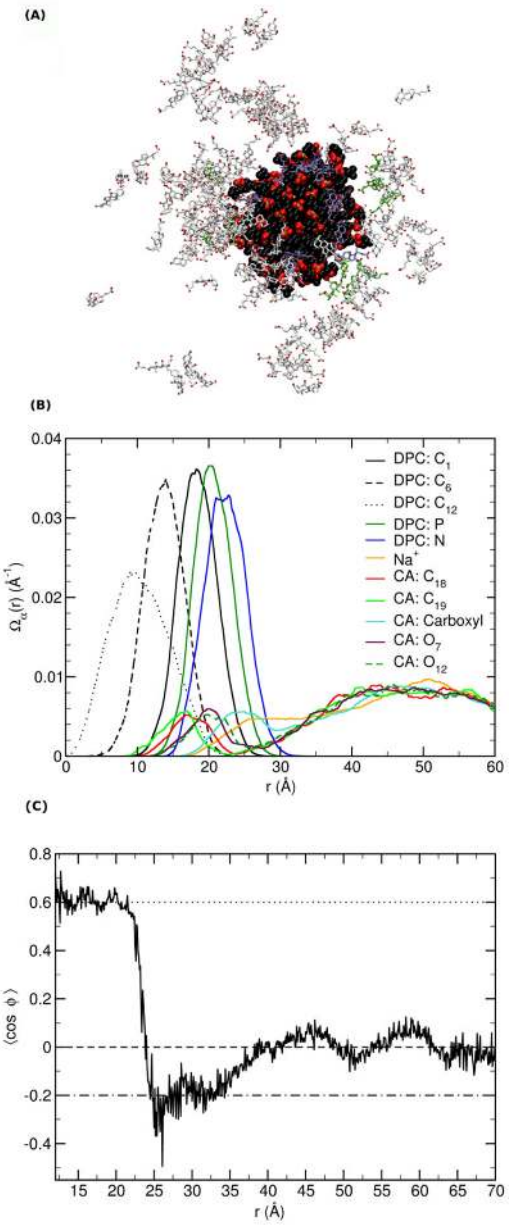

Figure 7.

(A) Snapshot of a DPC-CA micelle (center) and CA aggregates taken from simulation B. DPC molecules are depicted in space-filling model colored in black (carbon), red (oxygen), blue (nitrogen) and olive (phosphate). The CA molecules adsorbed onto the DPC micelle are colored in ice blue (carbon) and red (oxygen); those in the secondary shell (defined as non-adsorbed CA molecules containing a heavy atom within 8 Å of any DPC heavy atom) are in green and red, whereas the rest are colored in light gray. Water, counter ions and hydrogen atoms are not shown for clarity. (B) The probability distribution of selected atoms as a function of their distance from the center of mass of the mixed micelle.(C) C_{13} — C_{18} and C_{10} — C_{19} bond orientations as a function of distance from the center of mass of the mixed micelle.

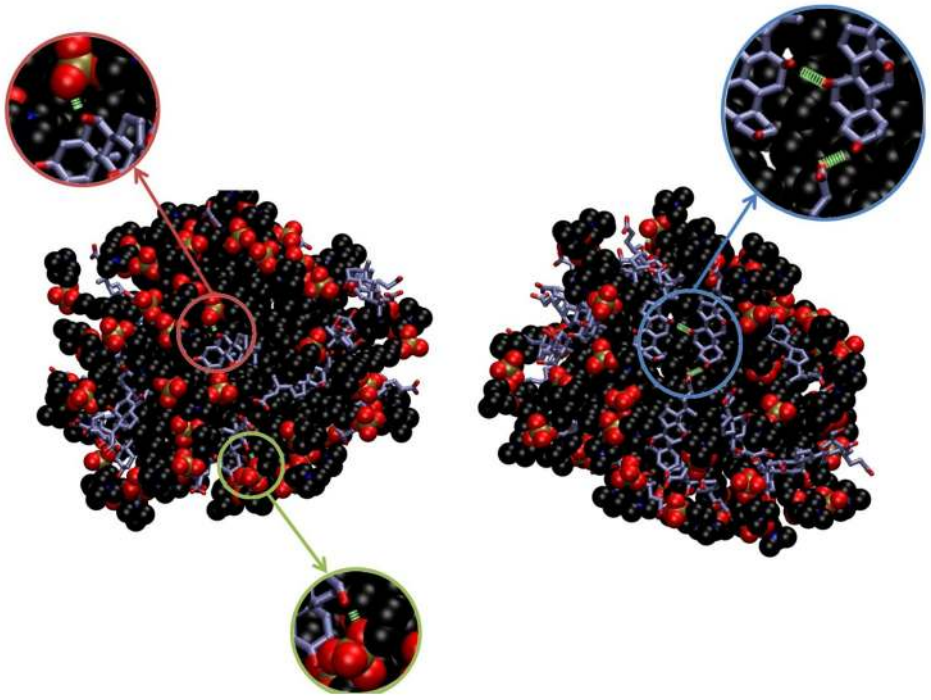

Figure 8.
Hydrogen bonds (green dashed line) between CA hydroxyl and DPC phosphate groups (left) and between adsorbed CA molecules (right).

Langmuir. Author manuscript; available in PMC 2011 August 17.

Table 1

Summaries of Simulation Performed.

Simulation Number	DPC-to-CA ratio	[DPC] (mM)	[CA] (mM)	System Size (atoms)	Simulation Length (ns)
A	0.00	0	270.30	38838	50
B	0.33	94.4	283.1	111657	50
C	1.00	110.2	110.2	94250	100
C′	1.00	110.6	110.6	94151	75
C″	1.00	249.5	249.5	42498	50
D	2.00	259.4	129.7	40428	50
E	4.00	264.6	66.2	39393	50

The DPC and CA concentrations, DPC-to-CA ratios, system sizes and simulation lengths are listed. Simulation A was started from a water box containing 60 CA molecules randomly distributed whereas simulations B–E contained a preformed DPC micelle of 60 DPC surfactants in a water box into which 180 (B), 60 (C), 30 (D) and 15 (E) CA molecules were added, as described in the methods.